

# CountCluster: Training-Free Object Quantity Guidance with Cross-Attention Map Clustering for Text-to-Image Generation

Joohyeon Lee\* Jin-Seop Lee\* Jee-Hyong Lee†  
 Sungkyunkwan University, Suwon, South Korea  
 {leeju001, wlstjq0602, john}@skku.edu

## Abstract

Text-to-image diffusion models have achieved substantial advances in generating visual content. However, these models often fail to produce the intended number of objects specified in a prompt. Several studies tried to address this limitation by incorporating external counting tools or designing additional object-specific control mechanisms, but these approaches still struggle with consistent quantity alignment and introduce extra computational overhead. To address this problem without relying on additional training or external modules, we propose CountCluster, a simple and effective method for accurate object-count control. We observe that the object count is strongly influenced by the object cross-attention map (CAM) at the first denoising timestep. Based on this observation, our method aligns early-timestep CAMs with the intended object count. Our method extracts high-activation regions from the object CAM, clusters them into the desired number of groups, and constructs a continuous CAM-aware target map using Gaussian smoothing. By minimizing the KL divergence between the CAM and the target object map at the first denoising timestep, the model is guided to form activation regions corresponding to the specified object count. Our method enables the model to reflect the intended object count across a wide range of complex and diverse prompt settings while preserving high image quality, all without training or reliance on external modules. Code will be released at <https://github.com/JoohyeonL22/CountCluster>

## 1. Introduction

Generative models have led to remarkable progress in the field of text-to-image generation, where visual content is synthesized solely from natural language descriptions. While early approaches were based on GANs [9, 19, 31], diffusion models [8, 16, 36] have recently demonstrated su-

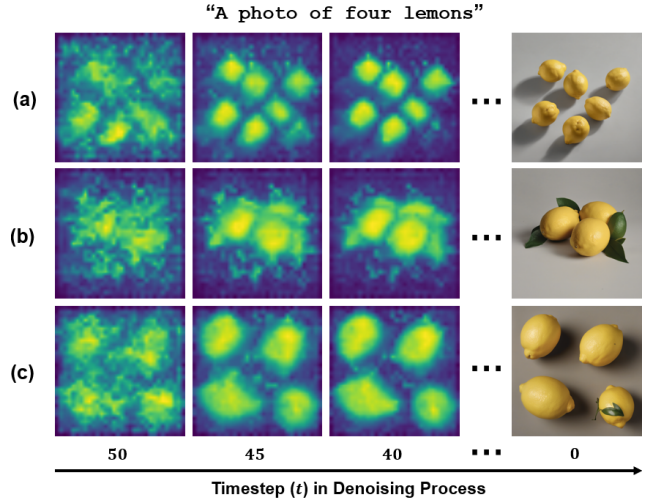


Figure 1. Generated images using SDXL [30] for the prompt “A photo of four lemons”. Each example, generated under the same conditions with different seeds, shows the cross-attention maps of “lemons” at timesteps  $t = 50, 45, 40$  together with the final image at  $t = 0$ . (a) and (b) are failure cases with incorrect instance counts, while (c) is a successful case with the correct number of instances. It can be observed that the positions and number of instances are mostly determined at the early timesteps of the denoising process.

perior performance in terms of image quality and diversity. With the development of diffusion models, various applications including image synthesis [10, 33, 37], inpainting [7, 23, 24, 26], and visual editing [4, 20, 38] have been increasingly adopted in practical scenarios. This trend highlights a growing need to generate images that faithfully reflect the user’s intent, including the specified number of instances. However, diffusion models still struggle to generate images that correctly reflect the exact number of instances of each object described in the input text (e.g., “a photo of four lemons”) [17, 28, 40].

Recently, several studies have been conducted to address the limitations of reflecting object quantity in generated images. Existing approaches can be categorized into

\*Equal contribution

†Corresponding author

two types: iterative refinement-based methods and quantity-representation guided methods. Iterative refinement-based approaches [3, 18] estimate the number of object instances during the image generation process, and then either regenerate the image or iteratively refine it while re-estimating the count. Quantity-representation guided approaches [42, 43] encode quantity information either by defining new tokens that learn quantity representations or by extracting latent vectors that control the number of instances. Then, they utilize these quantity representations to guide the generation of other object categories with the same count. These approaches show improvements over a naive Stable Diffusion [30, 36], however, they still struggle to generate images with the exact number of objects. Importantly, they overlook the most critical factor for quantity control—the number of instances in the generated image is mostly determined during the early timesteps of the diffusion process.

For diffusion models, highly activated regions in the object cross-attention map (CAM), which indicate strong attention to the corresponding object token, are strongly correlated with the object locations in the generated image [12]. As shown in the cross-attention maps for “lemons” token in Fig. 1, the positions and number of objects are largely determined at the early timesteps of the generation process. When the number of clusters of highly activated regions in the object cross-attention map at early timesteps exceeds the object quantity specified in the input prompt, the generated image tends to contain more objects, as shown in Fig. 1(a). In contrast, when the boundaries between activated regions are ambiguous and overlapping, some objects may be merged during the generation process, resulting in fewer object instances being generated, as shown in Fig. 1(b). Therefore, to ensure that the generated image reflects the object quantity specified in the text prompt, the cross-attention map at the early timesteps should form clusters of highly activated regions that exactly correspond to the intended object count, and each region should be clearly separated, as shown in Fig. 1(c).

In addition, existing methods [3, 18, 42, 43] rely on external tools such as object counting and layout generation, or require training quantity-representations to encode instance count information. As a result, they incur substantial computational costs and time overhead, making practical deployment of quantity control techniques challenging. Therefore, it is necessary to reflect quantity information without requiring additional modules and training.

In this paper, we propose *CountCluster*, a method that generates the intended number of object instances without relying on any external tools or additional training. We found that clustering the object cross-attention map (CAM) at the first denoising timestep effectively controls the number of generated objects to match the intended count. We also observed that the clustering process should be guided

by the originally high-activation regions in the CAM to reflect the intended object count. Based on these observations, our method updates the latent representation at the first denoising timestep, guiding the object CAM to form spatially separated activation clusters that match the intended number of objects. To achieve this, we construct a CAM-aware target object map by extracting and clustering the high-activation regions from the original CAM, ensuring that each cluster corresponds to a single intended object. We then apply a Gaussian filter to the clustered map to obtain a continuous target distribution and compute the KL divergence between this distribution and the actual object CAM. During the first denoising timestep, we minimize this KL divergence loss to guide the CAM toward spatially distinct activation regions that reflect the specified object count.

To demonstrate the effectiveness of our method, we conduct experiments across diverse prompt cases, validating its robustness and broad applicability. The method consistently improves instance count accuracy over existing approaches. Our approach achieves strong performance by ensuring the object CAM at the initial denoising timestep is well separated according to the intended object count, without requiring any additional training or external modules, ensuring both efficiency and ease of application.

## 2. Related Work

### 2.1. Image Generation with Accurate Object Count

Although diffusion-based text-to-image models have achieved remarkable progress in visual quality and semantic alignment, they still struggle to accurately reflect the number of objects explicitly specified in prompts [17, 28]. To address this limitation, various approaches have been proposed. Iterative refinement methods [3, 18] estimate the number of object instances during the image generation process, and then iteratively refine or regenerate the image based on the estimated count. Another line of research focuses on explicitly incorporating quantity information into the generation process [42, 43]. These methods either introduce count tokens to directly train models for quantity control or adopt quantity-representation guided approaches, which extract numerical embeddings from the CLIP [32] feature space to encode object count information. Nevertheless, these approaches still struggle with accurate object counting and even require additional training or external modules.

### 2.2. Latent Optimization via Attention Guidance

Training-free latent optimization has been actively explored to precisely control the outputs of pretrained text-to-image generation models. In particular, various approaches leveraging cross-attention maps have been proposed. Methods leveraging cross-attention maps are grounded in a simple

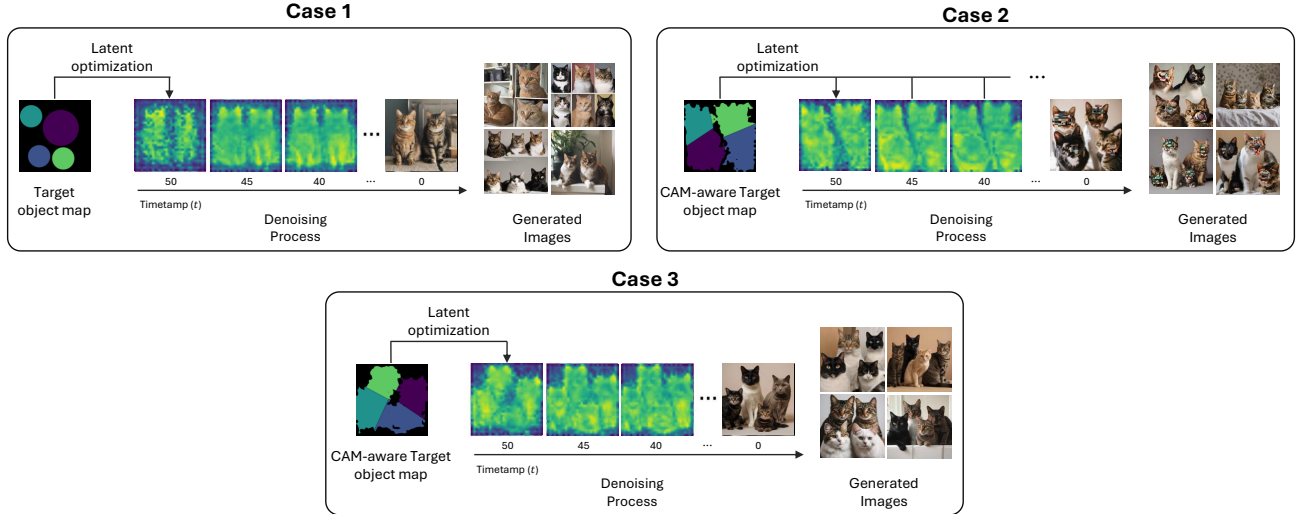


Figure 2. Comparison of three latent optimization settings for controlling object quantity.

observation: regions with high attention scores for a given text token tend to represent its concept more strongly in the generated image [12]. Building on this insight, Attend-and-Excite [6] addresses the problem of subject neglect—where objects mentioned in the text prompt fail to appear in the generated image. It introduces a loss function based on normalized cross-attention scores, which is used to iteratively optimize the latent representation. Subsequently, several studies [1, 11, 25, 34, 39] have proposed similar latent optimization strategies, primarily aiming to mitigate subject neglect by reinforcing attention to specific tokens. Such methods have the advantage of regulating object presence without modifying the pretrained diffusion model. However, they primarily focus on the binary presence or absence of objects, and still struggle to control quantitative attributes such as object count.

### 3. Proposed Method

#### 3.1. Preliminaries

**Overview.** We propose CountCluster, a method that generates the intended number of object instances without relying on any external tools or additional training. Our method updates the latent representation at the first denoising timestep, guiding the object CAM to form spatially separated activation clusters that match the intended number of objects. We first introduce the background of attention-guided latent optimization in Sec. 3.1. Then, we present the motivations for generating objects that accurately match the intended count in Sec. 3.2 and introduce our proposed method in Sec. 3.3.

#### Background of Attention-Guided Latent Optimization.

Recent studies have revealed a strong correlation between

the object cross-attention map (CAM) and the presence of specific objects in generated images. Hertz et al. [12] observed that, for a text token  $y_i$ , higher attention regions in its object CAM  $A_c^{(y_i)}$  tend to more strongly represent the corresponding visual concept in the generated image. Building on this finding, several studies have proposed modifying CAMs to promote the emergence of desired objects and optimizing the latent representation accordingly [1, 11, 34]. These approaches design a loss function based on the object CAM to ensure that the object appears in the generated image, and iteratively update the latent variable  $\mathbf{z}_t$  to minimize the loss. To encourage the appearance of objects in the generated image, they generally perform latent optimization over multiple timesteps, typically during the early-to-middle stages of the denoising process. This process can be formulated as follows:

$$\mathbf{z}'_t \leftarrow \mathbf{z}_t - \alpha_t \cdot \nabla_{\mathbf{z}_t} \mathcal{L}(A_c^{(y_i)}) \quad (1)$$

where  $\mathbf{z}_t$  denotes the latent representation at timestep  $t$ , and  $\alpha_t$  is a scaling factor that controls the magnitude of the gradient step.

#### 3.2. Motivation

Recent research has shown that regions with higher activation in the object cross-attention map (CAM) are strongly correlated with the emergence of corresponding objects in generated images. Building on this observation, we analyze how the object CAM can be effectively leveraged to control object quantities during the denoising process.

Figure 2 shows the results when the KL divergence between the object CAM and the target object map, which is clustered according to the intended number of objects, is used as a loss function for latent optimization. When this

KL divergence is minimized, the model tends to generate images that more strongly represent the corresponding visual concepts. We conduct experiments under three different cases. In case 1, randomly distributed clusters are used as the target object map, and latent optimization is applied only at the initial denoising timestep ( $t = 50$ ). In case 2, a CAM-aware target object map is used, and latent optimization is performed across multiple timesteps (e.g., from 50 to 25). In case 3, we apply CAM-aware latent optimization only once at the initial denoising step.

In case 1, randomly distributed clusters fail to reflect the intended object count. Because the random layout provides no meaningful spatial prior, the optimization gradients in latent space are misaligned with the diffusion model’s natural denoising process. In contrast, case 2, which uses CAM-aware target object maps, successfully reflects the intended object count, showing that CAM-guided latent optimization can achieve quantity control without additional training. However, in this setting, most generated objects tend to degrade image quality. This occurs because the appearance of objects in diffusion models is primarily determined in the very early timesteps, and repeatedly applying optimization in later timesteps interferes with this natural formation process. In case 3, where latent optimization is performed only at the first denoising timestep, the generated images accurately reflect the intended count while maintaining natural structure and high visual quality. Optimizing only at the initial timestep focuses on aligning the core semantic regions, thereby preserving both object count accuracy and overall image quality.

These experimental results lead to two key observations. First, optimizing the latent representation such that the object CAM forms distinct clusters at the initial denoising timestep provides the most effective control over object quantity. Second, the clustering process should be guided to form around the originally high-activation regions in the object CAM, ensuring that the semantic focus of each object is preserved while maintaining alignment with the intended count. Based on these observations, we optimize the latent representation at the first denoising timestep, guiding the object CAM to form clearly separated activation clusters that match the intended number of objects.

### 3.3. CountCluster

Based on the above observations, we propose *CountCluster*, a method that generates the intended number of object instances without relying on any external tools or additional training. During the first denoising timestep, we optimize the latent representation to minimize the KL divergence between the object CAM and a CAM-aware target object map, encouraging the model to produce spatially distinct activations that align with the intended object count.

To effectively reflect the intended count, the target ob-

ject map should cluster the high-activation regions into the specified number of groups. To achieve this, we utilize the high-activation regions from the object CAM. We first extract regions whose activation scores exceed a predefined threshold and then cluster them to construct the CAM-aware target object map. However, this target map is still binary, whereas cross-attention maps in diffusion models exhibit continuous-valued activations. To address this, we apply a Gaussian filter to the target map to obtain a continuous-valued target distribution. Based on this extracted CAM-aware target object map, we compute the CountCluster loss to guide the object CAM to produce clearly separated activation clusters. This approach enables the model to reflect the intended count while preserving high image quality, even in a fully training-free manner and without any external modules.

#### 3.3.1. CAM-aware Target Object Map Extraction

**High-Activation Region Extraction and Clustering.** To precisely control the number of generated objects, it is essential that the clustering process is guided to form around the originally high-activation regions. To achieve this, we construct a CAM-aware target object map. We begin by restricting control to regions in the object CAM that exhibit sufficiently high-activation values. Specifically, we apply an attention threshold  $\tau$  to the normalized CAM (we set  $\tau = 0.35$ ) to generate a mask and extract candidate regions that are likely to contribute to object formation. These high-activation regions serve as the basis for determining the cluster centers, and our method guides object generation around these regions.

Our target map aims to obtain  $k$  separated regions corresponding to the  $k$  intended objects. To this end, we employ a connected component labeling algorithm to count the number of contiguous subregions and adjust this number to match the target object count  $k$ . If the number of regions exceeds  $k$ , we sequentially remove smaller regions. Conversely, if the number of regions is insufficient, we subdivide the largest region using a K-means-based partitioning and exclude the boundary between the two clusters from the mask, resulting in two independent regions. By iteratively applying this process, we obtain  $k$  control regions that correspond to the intended object count while preserving the overall structure of the original CAM. Additional implementation details are provided in the Appendix.

**Continuous CAM-aware Target Map Construction.** In the previous step, we extracted  $k$  high-activation cluster regions from the object CAM. However, the resulting target map is still a binary mask, which differs from the continuous activation patterns observed in diffusion models. To obtain a continuous target distribution, we apply a Gaussian filter to the clustered object map.

For each cluster, we construct a 2D Gaussian whose value is 1 at the cluster center and  $\tau$  at the cluster boundary. The variance  $\sigma$  is determined by the distance  $r$  between the center and boundary:

$$\sigma = \sqrt{\frac{r^2}{-2\log(\tau)}}, \quad T(\mathbf{x}) = \exp\left(-\frac{|\mathbf{x} - \boldsymbol{\mu}|^2}{2\sigma^2}\right). \quad (2)$$

Here,  $T(\mathbf{x})$  denotes the continuous CAM-aware target object map,  $\boldsymbol{\mu}$  represents the cluster center, and  $\mathbf{x}$  is the coordinate of each patch in the attention map. This Gaussian smoothing produces coherent activation regions with clear separation between clusters, enabling the activation map to better reflect the intended object count.

### 3.3.2. Latent Optimization with CountCluster Loss

To guide the object CAM toward forming clearly separated activation clusters, we introduce the CountCluster loss, which consists of two components: an appearance loss  $\mathcal{L}_{\text{appear}}$  and a separation loss  $\mathcal{L}_{\text{sep}}$ . The appearance loss encourages the object CAM to align with the CAM-aware target map composed of  $k$  well-separated clusters, each corresponding to one intended object. The separation loss suppresses activation outside the cluster regions, maintaining clear boundaries between objects and keeping the object CAM focused on the intended object areas.

To align the object CAM with the target map, we measure the discrepancy between the actual CAM  $A_c(x)$  and the target object map  $T_j(x)$  using KL divergence [21]. The appearance loss is formulated as:

$$\mathcal{L}_{\text{appear}} = \frac{1}{\sqrt{k}} \sum_{j=1}^k D_{\text{KL}}(T_j(x) \| A_c(x)) \quad (3)$$

where the KL divergence is computed independently for each of the  $k$  clusters. Since the total KL value naturally increases with the number of clusters  $k$ , we normalize it by  $\sqrt{k}$  to maintain a consistent scale across different object counts. To suppress unnecessary activation outside the clusters, we restrict attention values in non-target regions so that they do not exceed the threshold  $\tau$ . Since a direct max operation is non-differentiable, we employ a smooth approximation using the LogSumExp function:

$$\mathcal{L}_{\text{sep}} = \text{ReLU}\left(\text{LogSumExp}(A_c^{(y_i)} - \tau)\right) \quad (4)$$

This formulation suppresses overly high-activation outside the cluster mask and guides the CAM to remain focused within object-relevant regions. Finally, the total loss is consisted of the appearance and separation losses, and applied at the first denoising timestep to update the latent representation:

$$\mathcal{L}_{\text{total}} = \mathcal{L}_{\text{appear}} + \mathcal{L}_{\text{sep}}, \quad (5)$$

$$\mathbf{z}'_t \leftarrow \mathbf{z}_t - \alpha_t \cdot \nabla_{\mathbf{z}_t} \mathcal{L}_{\text{total}} \quad (6)$$

## 4. Experiments

### 4.1. Experimental setup

**Benchmarks.** To quantitatively evaluate the model’s ability to control object quantities, we utilized various quantity-aware prompt sets following previous object-counting studies [3, 18]. Each prompt follows the template *a photo of [count] [object]*, where *[count]* is a number word ranging from *two* to *ten*. This design allows systematic evaluation across diverse object categories and a range of object counts. To demonstrate the method’s robustness and adaptability across diverse prompt conditions, we also evaluate the proposed method on more complex scenarios, including coiled and elongated objects, occluded scenes, and various natural backgrounds, as discussed in Sec. 5.2.

**Baselines.** We compare our method against five baseline approaches, including those specifically designed for object quantity control. The baselines are implemented on either SD2.1 [36] or SDXL [30], and results are reported separately according to the underlying diffusion backbone. Counting-Guidance [18] operates on SD2.1, whereas Zafar et al. [42] and CountGen [3] are built on SDXL. Since our method requires no architectural changes, training, or auxiliary modules, it can be directly applied to both backbones. For fair comparison, we therefore evaluate and report our method on both SD2.1 and SDXL alongside their corresponding baselines.

**Metrics.** For evaluation, we assess the proposed method from two complementary perspectives: object-count accuracy and image quality. For counting evaluation, we employ two independent assessment tools—CountGD [2], an object-counting model built upon Grounding DINO [22], and the TIFA framework [17], which uses GPT-4o mini [27] as its Visual Question Answering (VQA) backbone. Both tools automatically estimate the number of object instances in each generated image, and the results are compared with the quantities specified in the prompts to measure quantitative accuracy. For image-quality evaluation, we adopt CLIP-Score [14] and ImageReward [41] to assess visual-textual quality and human-preference alignment.

### 4.2. Qualitative Results

Figure 3 presents a qualitative comparison between our method and existing baselines. To evaluate how models respond to changes in object count, we generated images from prompts that differ only in the specified number while keeping the initial latent fixed. Our method reliably reflects the intended quantity (e.g., five turtles  $\rightarrow$  six turtles) without disrupting scene composition or visual coherence. In contrast, baseline models often fail to adjust the count or generate duplicated and overlapping objects.

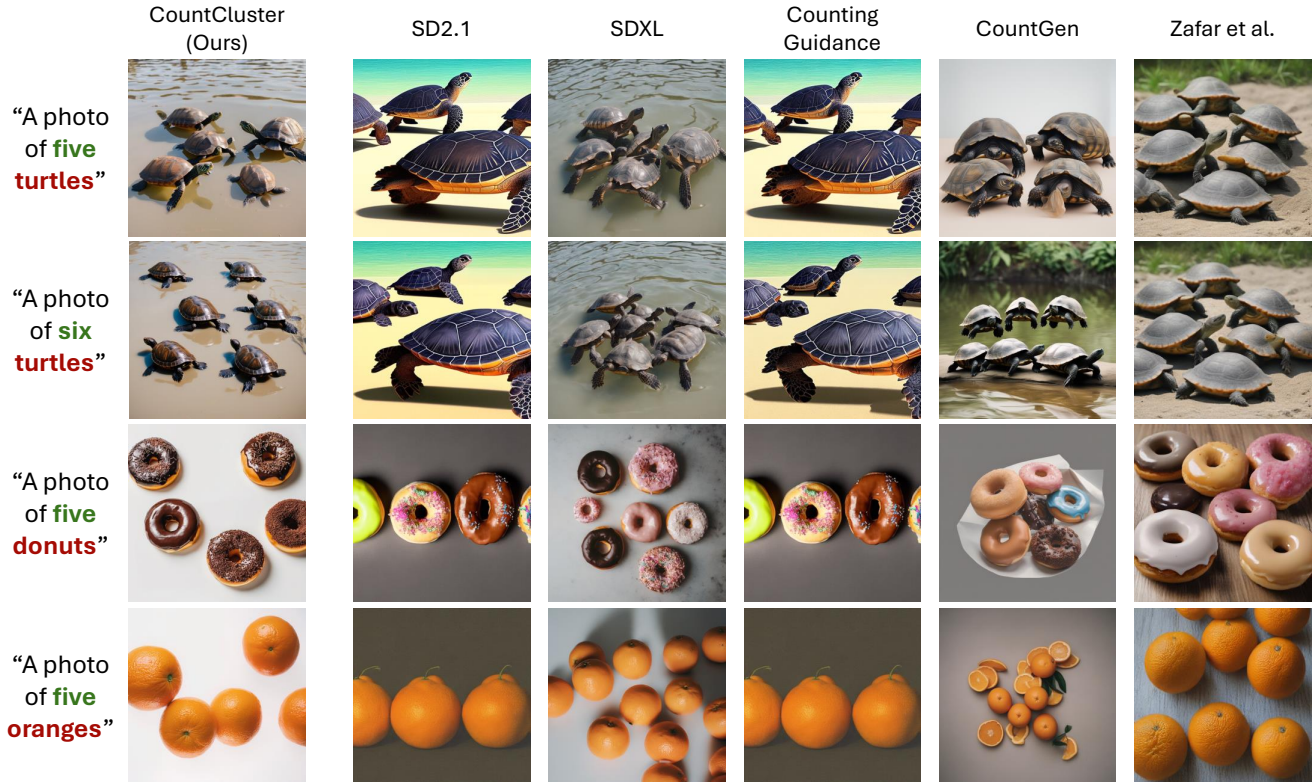


Figure 3. The first two rows illustrate cases where only the object quantity in the prompt is changed while keeping the random seed. The last two rows show results where only the object category (e.g., “donuts” → “oranges”) is changed under the same random seed.

Method	CountGD [2]			TIFA [17]	
	Acc. (↑)	MAE (↓)	RMSE (↓)	Counting (↑)	Appearing (↑)
SD2.1 [36]					
Naive SD2.1 [36]	24.56	1.990	3.127	72.15	99.75
Counting-Guidance [18]	24.95	1.885	<b>2.982</b>	71.57	99.51
Ours	<b>33.33</b>	<b>1.791</b>	3.282	<b>75.76</b>	<b>99.26</b>
SDXL [30]					
Naive SDXL [30]	27.88	5.045	9.302	73.01	<b>99.75</b>
Zafar et al. [42]	25.93	1.815	2.924	76.62	99.01
CountGen [3]	46.20	1.661	3.562	76.48	97.28
Ours	<b>55.75</b>	<b>0.821</b>	<b>1.849</b>	<b>79.51</b>	99.26

Table 1. Experimental Results on SD2.1 and SDXL using CountGD [2] and TIFA [17]. CountGD measures numerical accuracy using Accuracy (↑), MAE (↓), and RMSE (↓), while TIFA evaluates text–image consistency through Counting (↑) and Appearing (↑) scores.

Our method also maintains accurate instance counts across diverse object categories (e.g., five donuts → five oranges). These results demonstrate that our method achieves robust quantity control through attention-based clustering rather than relying solely on pretrained model priors. Overall, the qualitative results show that our method preserves visual fidelity while producing images that adhere to the quantities specified in the prompt.

### 4.3. Quantitative Results

**Object Count Accuracy.** Table 1 presents the quantitative comparison on SD2.1 and SDXL using CountGD [2] and TIFA [17]. Across all metrics—including Accuracy, MAE, RMSE, and VQA-based counting consistency—our proposed *CountCluster* outperforms existing approaches. For SDXL, our method also substantially outperforms numerical precision over prior methods. In addition, the

Method	Image Quality	
	CLIPScore ( $\uparrow$ )	ImageReward ( $\uparrow$ )
SD2.1 [36]		
Naive SD2.1 [36]	0.265	0.780
Counting Guidance [18]	0.265	0.768
Ours	0.265	0.744
SDXL [30]		
Naive SDXL [30]	0.268	0.568
Zafar et al. [42]	0.267	0.921
CountGen [3]	0.268	0.550
Ours	0.262	0.563

Table 2. Comparison of image quality using CLIPScore [14] and ImageReward [41].

Method	Time (s)	Mem. (GB)	Training	External
SD2.1 [36]				
Naive SD2.1 [36]	5.89	7	$\times$	$\times$
Counting Guidance [18]	21.27	14	$\times$	$\checkmark$
Ours	9.14	7	$\times$	$\times$
SDXL [30]				
Naive SDXL [30]	13.32	15	$\times$	$\times$
Zafar et al. [42]	9.07	16 (26*)	$\checkmark$	$\times$
CountGen [3]	88.04	71	$\times$	$\checkmark$
Ours	36.38	18	$\times$	$\times$

Table 3. Inference time and peak GPU memory are measured per generated image on an RTX 3090. ‘‘Training’’ indicates whether additional model fine-tuning is required, and ‘‘External’’ denotes reliance on auxiliary counting or detection modules.

TIFA results confirm that our method maintains strong text–image alignment. These improvements indicate that aligning early-timestep attention clustering effectively enhances quantitative faithfulness between prompt and image without requiring extra training.

**Image Quality.** Table 2 reports the image quality evaluation using CLIPScore [14] and ImageReward [41]. Although our approach focuses solely on quantity control, it maintains comparable visual quality to baseline models. The results show that our method achieves nearly identical CLIPScore while exhibiting only minor variation in ImageReward, confirming that quantitative control does not compromise perceptual quality or prompt-image coherence.

**Efficiency Analysis.** Table 3 compares inference time, GPU memory, and dependency overhead. Our method introduces only minimal computational cost compared to base diffusion models, while avoiding any additional training or external counting modules. Unlike prior methods such as CountGen, which require up to 71 GB of memory and multi-stage regeneration, our method operates in a single

Method	CountGD		
	Acc. ( $\uparrow$ )	MAE ( $\downarrow$ )	RMSE ( $\downarrow$ )
Naive SDXL	27.88	5.045	9.302
Case 1	29.82	3.353	7.137
Case 2	33.33	54.493	114.855
w/o $L_{appear}$	20.66	6.544	12.503
w/o $L_{sep}$	<u>42.88</u>	<u>0.949</u>	<b>1.553</b>
Ours	<b>55.75</b>	<b>0.821</b>	<u>1.849</u>

Table 4. Ablation study on key components of CountCluster.

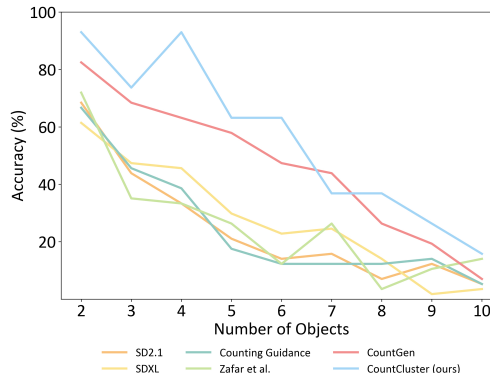


Figure 4. Accuracy comparison across different object counts. It illustrates the model performance as the number of objects specified in the prompt increases from 2 to 10.

forward denoising pass with negligible overhead. Overall, our method achieves accurate and efficient object-count control while remaining fully training-free and independent of external modules.

## 5. Analysis

### 5.1. Ablation Study

Table 4 shows the contribution of each component in CountCluster. Cases 1 and 2 follow the same settings described in Sec. 3.2. Using a random Gaussian target cluster map (Case 1) yields only modest improvement over the naive model, indicating that the target distribution must align with meaningful high-activation regions. Applying latent optimization across multiple early timesteps (Case 2) leads to highly unstable predictions and large RMSE values, confirming that optimization beyond the first denoising step disrupts the model’s natural generation trajectory.

We further examine the contribution of each loss component in the CountCluster loss. Removing the appearance term prevents the object CAM from aligning with the CAM-aware target map, weakening cluster formation and causing the model to frequently underestimate the object count. In contrast, removing the separation term allows activation to spread beyond the target regions, producing merged or duplicated attention clusters that lead to over-counting. Using

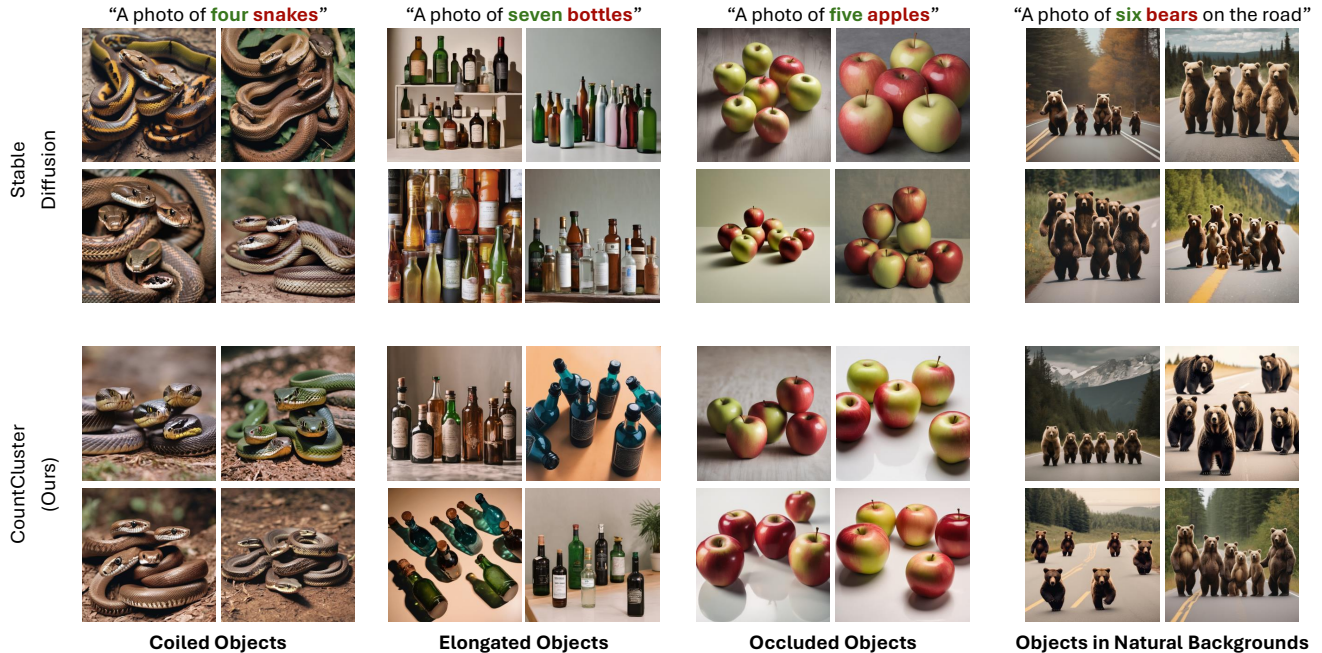


Figure 5. Qualitative results on complex object configurations, including coiled, elongated, occluded, and objects in natural backgrounds.

both terms together yields the most stable cluster structure and the best quantitative performance, indicating that appearance alignment and activation suppression are both essential for reliable quantity control.

## 5.2. Discussions

**Accuracy via Object Counts.** Figure 4 compares the counting accuracy of different methods across varying object counts. All methods show reduced accuracy as the number of objects increases, reflecting the challenge of maintaining instance separation in crowded scenes. Our method achieves consistently higher accuracy with a smoother degradation curve, matching CountGen at two objects and surpassing all baselines beyond three. Notably, accuracies peak around four and nine objects, likely due to regular spatial layouts (e.g.,  $2 \times 2$  or  $3 \times 3$  grids) that diffusion models naturally favor. These results demonstrate that our method maintains quantitative consistency even under complex spatial configurations.

**Qualitative Results on Complex Prompts.** Figure 5 presents qualitative results on complex prompts. The proposed method maintains accurate quantity control under diverse spatial configurations and visual contexts, including coiled, elongated, occluded, and natural-scene objects. Even when instances overlap or blend into the background, our method effectively separates attention regions, preventing merging or omission. Since latent optimization is performed only at the first denoising timestep, objects are natu-

rally distributed while preserving spatial consistency guided by the target cluster map. These results confirm that our approach achieves visually coherent and robust quantity control across challenging scenarios.

## 6. Conclusion

In this work, we showed that object quantity in diffusion models is strongly influenced by the object cross-attention map (CAM) at the first denoising timestep. Leveraging this insight, we introduced CountCluster, a training-free approach that controls object count without external modules. By clustering high-activation CAM regions and constructing a continuous CAM-aware target map, the method guides early-timestep CAMs toward activation patterns that match the intended object count through a KL-based optimization. CountCluster requires no training or architectural changes yet effectively aligns generated images with the specified number of objects while maintaining visual quality across diverse prompt settings.

## References

- [1] Aishwarya Agarwal, Srikrishna Karanam, K J Joseph, Apoorv Saxena, Koustava Goswami, and Balaji Vasani. A-star: Test-time attention segregation and retention for text-to-image synthesis. In *Proceedings of the IEEE/CVF International Conference on Computer Vision (ICCV)*, pages 2283–2293, 2023. 3
- [2] Niki Amini-Naieni, Tengda Han, and Andrew Zisserman. Countgd: multi-modal open-world counting. In *Proceedings*

- of the 38th International Conference on Neural Information Processing Systems, Red Hook, NY, USA, 2025. Curran Associates Inc. 5, 6, 13, 15
- [3] Lital Binyamin, Yoad Tewel, Hilit Segev, Eran Hirsch, Royi Rassin, and Gal Chechik. Make it count: Text-to-image generation with an accurate number of objects. *arXiv preprint arXiv:2406.10210*, 2024. 2, 5, 6, 7, 13, 15
- [4] Mingdeng Cao, Xintao Wang, Zhongang Qi, Ying Shan, Xiaohu Qie, and Yinqiang Zheng. Masactrl: Tuning-free mutual self-attention control for consistent image synthesis and editing. In *Proceedings of the IEEE/CVF International Conference on Computer Vision (ICCV)*, pages 22560–22570, 2023. 1
- [5] Yu Cao, Zengqun Zhao, Ioannis Patras, and Shaogang Gong. Temporal score analysis for understanding and correcting diffusion artifacts. In *Proceedings of the Computer Vision and Pattern Recognition Conference*, pages 7707–7716, 2025. 15
- [6] Hila Chefer, Yuval Alaluf, Yael Vinker, Lior Wolf, and Daniel Cohen-Or. Attend-and-excite: Attention-based semantic guidance for text-to-image diffusion models. *ACM Trans. Graph.*, 42(4), 2023. 3, 13
- [7] Guillaume Couairon, Jakob Verbeek, Holger Schwenk, and Matthieu Cord. Diffedit: Diffusion-based semantic image editing with mask guidance. In *The Eleventh International Conference on Learning Representations*, 2023. 1
- [8] Prafulla Dhariwal and Alex Nichol. Diffusion models beat gans on image synthesis. In *Proceedings of the 35th International Conference on Neural Information Processing Systems*, Red Hook, NY, USA, 2021. Curran Associates Inc. 1
- [9] Ian J. Goodfellow, Jean Pouget-Abadie, Mehdi Mirza, Bing Xu, David Warde-Farley, Sherjil Ozair, Aaron Courville, and Yoshua Bengio. Generative adversarial nets. In *Advances in Neural Information Processing Systems*. Curran Associates, Inc., 2014. 1
- [10] Shuyang Gu, Dong Chen, Jianmin Bao, Fang Wen, Bo Zhang, Dongdong Chen, Lu Yuan, and Baining Guo. Vector quantized diffusion model for text-to-image synthesis. In *Proceedings of the IEEE/CVF Conference on Computer Vision and Pattern Recognition (CVPR)*, pages 10696–10706, 2022. 1
- [11] Xiefan Guo, Jinlin Liu, Miaomiao Cui, Jiankai Li, Hongyu Yang, and Di Huang. Initno: Boosting text-to-image diffusion models via initial noise optimization. In *Proceedings of the IEEE/CVF Conference on Computer Vision and Pattern Recognition (CVPR)*, pages 9380–9389, 2024. 3
- [12] Amir Hertz, Ron Mokady, Jay Tenenbaum, Kfir Aberman, Yael Pritch, and Daniel Cohen-or. Prompt-to-prompt image editing with cross-attention control. In *The Eleventh International Conference on Learning Representations*, 2023. 2, 3
- [13] Jack Hessel, Ari Holtzman, Maxwell Forbes, Ronan Le Bras, and Yejin Choi. CLIPScore: A reference-free evaluation metric for image captioning. In *Proceedings of the 2021 Conference on Empirical Methods in Natural Language Processing*, pages 7514–7528, Online and Punta Cana, Dominican Republic, 2021. Association for Computational Linguistics. 14
- [14] Jack Hessel, Ari Holtzman, Maxwell Forbes, Ronan Le Bras, and Yejin Choi. Clipscore: A reference-free evaluation metric for image captioning, 2022. 5, 7, 15
- [15] Jonathan Ho and Tim Salimans. Classifier-free diffusion guidance, 2022. 13
- [16] Jonathan Ho, Ajay Jain, and Pieter Abbeel. Denoising diffusion probabilistic models. In *Advances in Neural Information Processing Systems*, pages 6840–6851. Curran Associates, Inc., 2020. 1
- [17] Yushi Hu, Benlin Liu, Jungo Kasai, Yizhong Wang, Mari Ostendorf, Ranjay Krishna, and Noah A. Smith. Tifa: Accurate and interpretable text-to-image faithfulness evaluation with question answering. In *Proceedings of the IEEE/CVF International Conference on Computer Vision (ICCV)*, pages 20406–20417, 2023. 1, 2, 5, 6, 13, 15
- [18] Wonjun Kang, Kevin Galim, Hyung Il Koo, and Nam Ik Cho. Counting guidance for high fidelity text-to-image synthesis. In *2025 IEEE/CVF Winter Conference on Applications of Computer Vision (WACV)*, pages 899–908. IEEE, 2025. 2, 5, 6, 7, 13, 15
- [19] Tero Karras, Samuli Laine, and Timo Aila. A style-based generator architecture for generative adversarial networks. In *Proceedings of the IEEE/CVF Conference on Computer Vision and Pattern Recognition (CVPR)*, 2019. 1
- [20] Bahjat Kawar, Shiran Zada, Oran Lang, Omer Tov, Huiwen Chang, Tali Dekel, Inbar Mosseri, and Michal Irani. Imagic: Text-based real image editing with diffusion models. In *Conference on Computer Vision and Pattern Recognition 2023*, 2023. 1
- [21] Solomon Kullback and Richard A Leibler. On information and sufficiency. *The Annals of Mathematical Statistics*, 22 (1):79–86, 1951. 5, 13
- [22] Shilong Liu, Zhaoyang Zeng, Tianhe Ren, Feng Li, Hao Zhang, Jie Yang, Qing Jiang, Chunyuan Li, Jianwei Yang, Hang Su, Jun Zhu, and Lei Zhang. Grounding dino: Marrying dino with grounded pre-training for open-set object detection. In *Computer Vision – ECCV 2024*, pages 38–55, Cham, 2025. Springer Nature Switzerland. 5
- [23] Andreas Lugmayr, Martin Danelljan, Andres Romero, Fisher Yu, Radu Timofte, and Luc Van Gool. Repaint: Inpainting using denoising diffusion probabilistic models. In *Proceedings of the IEEE/CVF Conference on Computer Vision and Pattern Recognition (CVPR)*, pages 11461–11471, 2022. 1
- [24] Chenlin Meng, Yutong He, Yang Song, Jiaming Song, Jiajun Wu, Jun-Yan Zhu, and Stefano Ermon. SDEdit: Guided image synthesis and editing with stochastic differential equations. In *International Conference on Learning Representations*, 2022. 1
- [25] Tuna Han Salih Meral, Enis Simsar, Federico Tombari, and Pinar Yanardag. Conform: Contrast is all you need for high-fidelity text-to-image diffusion models. In *Proceedings of the IEEE/CVF Conference on Computer Vision and Pattern Recognition (CVPR)*, pages 9005–9014, 2024. 3
- [26] Alexander Quinn Nichol, Prafulla Dhariwal, Aditya Ramesh, Pranav Shyam, Pamela Mishkin, Bob McGrew, Ilya Sutskever, and Mark Chen. GLIDE: Towards photorealistic image generation and editing with text-guided diffusion

models. In *Proceedings of the 39th International Conference on Machine Learning*, pages 16784–16804. PMLR, 2022. 1

- [27] OpenAI, :, Aaron Hurst, Adam Lerer, Adam P. Goucher, Adam Perelman, Aditya Ramesh, Aidan Clark, AJ Ostrow, Akila Welihinda, Alan Hayes, Alec Radford, Aleksander Madry, Alex Baker-Whitcomb, Alex Beutel, Alex Borzunov, Alex Carney, Alex Chow, Alex Kirillov, Alex Nichol, Alex Paino, Alex Renzin, Alex Tachard Passos, Alexander Kirillov, Alexi Christakis, Alexis Conneau, Ali Kamali, Allan Jabri, Allison Moyer, Allison Tam, Amadou Crookes, Amin Tootoochian, Amin Tootoonchian, Ananya Kumar, Andrea Vallone, Andrej Karpathy, Andrew Braunstein, Andrew Cann, Andrew Codispoti, Andrew Galu, Andrew Kondrich, Andrew Tulloch, Andrey Mishchenko, Angela Baek, Angela Jiang, Antoine Pelisse, Antonia Woodford, Anuj Gosalia, Arka Dhar, Ashley Pantuliano, Avi Nayak, Avital Oliver, Barret Zoph, Behrooz Ghorbani, Ben Leimberger, Ben Rossen, Ben Sokolowsky, Ben Wang, Benjamin Zweig, Beth Hoover, Blake Samic, Bob McGrew, Bobby Spero, Bogo Gertler, Bowen Cheng, Brad Lightcap, Brandon Walkin, Brendan Quinn, Brian Guarraci, Brian Hsu, Bright Kellogg, Brydon Eastman, Camillo Lugaresi, Carroll Wainwright, Cary Bassin, Cary Hudson, Casey Chu, Chad Nelson, Chak Li, Chan Jun Shern, Channing Conger, Charlotte Barette, Chelsea Voss, Chen Ding, Cheng Lu, Chong Zhang, Chris Beaumont, Chris Hallacy, Chris Koch, Christian Gibson, Christina Kim, Christine Choi, Christine McLeavey, Christopher Hesse, Claudia Fischer, Clemens Winter, Coley Czarnecki, Colin Jarvis, Colin Wei, Constantin Koumouzelis, Dane Sherburn, Daniel Kappler, Daniel Levin, Daniel Levy, David Carr, David Farhi, David Mely, David Robinson, David Sasaki, Denny Jin, Dev Valladares, Dimitris Tsipras, Doug Li, Duc Phong Nguyen, Duncan Findlay, Edede Oiwoh, Edmund Wong, Ehsan Asdar, Elizabeth Proehl, Elizabeth Yang, Eric Antonow, Eric Kramer, Eric Peterson, Eric Sigler, Eric Wallace, Eugene Brevdo, Evan Mays, Farzad Khorasani, Felipe Petroski Such, Filippo Raso, Francis Zhang, Fred von Lohmann, Freddie Sulit, Gabriel Goh, Gene Oden, Geoff Salmon, Giulio Starace, Greg Brockman, Hadi Salman, Haiming Bao, Haitang Hu, Hannah Wong, Haoyu Wang, Heather Schmidt, Heather Whitney, Heewoo Jun, Hendrik Kirchner, Henrique Ponde de Oliveira Pinto, Hongyu Ren, Huiwen Chang, Hyung Won Chung, Ian Kivlichan, Ian O’Connell, Ian O’Connell, Ian Osband, Ian Silber, Ian Sohl, Ibrahim Okuyucu, Ikai Lan, Ilya Kostrikov, Ilya Sutskever, Ingmar Kanitscheider, Ishaan Gulrajani, Jacob Coxon, Jacob Menick, Jakub Pachocki, James Aung, James Betker, James Crooks, James Lennon, Jamie Kiros, Jan Leike, Jane Park, Jason Kwon, Jason Phang, Jason Teplitz, Jason Wei, Jason Wolfe, Jay Chen, Jeff Harris, Jenia Varavva, Jessica Gan Lee, Jessica Shieh, Ji Lin, Jiahui Yu, Jiayi Weng, Jie Tang, Jieqi Yu, Joanne Jang, Joaquin Quinonero Candela, Joe Beutler, Joe Landers, Joel Parish, Johannes Heidecke, John Schulman, Jonathan Lachman, Jonathan McKay, Jonathan Uesato, Jonathan Ward, Jong Wook Kim, Joost Huizinga, Jordan Sitkin, Jos Kraaijeveld, Josh Gross, Josh Kaplan, Josh Snyder, Joshua Achiam, Joy Jiao, Joyce Lee, Juntang Zhuang, Justyn Harriman, Kai Fricke, Kai Hayashi, Karan Singhal, Katy Shi, Kavin Karthik, Kayla Wood, Kendra Rimbach, Kenny Hsu, Kenny Nguyen, Keren Gu-Lemberg, Kevin Button, Kevin Liu, Kiel Howe, Krithika Muthukumar, Kyle Luther, Lama Ahmad, Larry Kai, Lauren Itow, Lauren Workman, Leher Pathak, Leo Chen, Li Jing, Lia Guy, Liam Fedus, Liang Zhou, Lien Mamitsuka, Lilian Weng, Lindsay McCallum, Lindsey Held, Long Ouyang, Louis Feувrier, Lu Zhang, Lukas Kondraciuk, Lukasz Kaiser, Luke Hewitt, Luke Metz, Lyric Doshi, Mada Aflak, Maddie Simens, Madelaine Boyd, Madeleine Thompson, Marat Dukhan, Mark Chen, Mark Gray, Mark Hudnall, Marvin Zhang, Marwan Aljubeih, Mateusz Litwin, Matthew Zeng, Max Johnson, Maya Shetty, Mayank Gupta, Meghan Shah, Mehmet Yatbaz, Meng Jia Yang, Mengchao Zhong, Mia Glaese, Mianna Chen, Michael Janner, Michael Lampe, Michael Petrov, Michael Wu, Michele Wang, Michelle Fradin, Michelle Pokrass, Miguel Castro, Miguel Oom Temudo de Castro, Mikhail Pavlov, Miles Brundage, Miles Wang, Minal Khan, Mira Murati, Mo Bavarian, Molly Lin, Murat Yesildal, Nacho Soto, Natalia Gimelshein, Natalie Cone, Natalie Staudacher, Natalie Summers, Natan LaFontaine, Neil Chowdhury, Nick Ryder, Nick Stathas, Nick Turley, Nik Tezak, Niko Felix, Nithanth Kudige, Nitish Keskar, Noah Deutsch, Noel Bundick, Nora Puckett, Ofir Nachum, Ola Okelola, Oleg Boiko, Oleg Murk, Oliver Jaffe, Olivia Watkins, Olivier Godement, Owen Campbell-Moore, Patrick Chao, Paul McMillan, Pavel Belov, Peng Su, Peter Bak, Peter Bakkum, Peter Deng, Peter Dolan, Peter Hoeschele, Peter Welinder, Phil Tillet, Philip Pronin, Philippe Tillet, Prafulla Dhariwal, Qiming Yuan, Rachel Dias, Rachel Lim, Rahul Arora, Rajan Troll, Randall Lin, Rapha Gontijo Lopes, Raul Puri, Reah Miyara, Reimar Leike, Renaud Gaubert, Reza Zamani, Ricky Wang, Rob Donnelly, Rob Honsby, Rocky Smith, Rohan Sahai, Rohit Ramchandani, Romain Huet, Rory Carmichael, Rowan Zellers, Roy Chen, Ruby Chen, Ruslan Nigmatullin, Ryan Cheu, Saachi Jain, Sam Altman, Sam Schoenholz, Sam Toizer, Samuel Miserendino, Sandhini Agarwal, Sara Culver, Scott Ethersmith, Scott Gray, Sean Grove, Sean Metzger, Shamez Hermani, Shantanu Jain, Shengjia Zhao, Sherwin Wu, Shino Jomoto, Shirong Wu, Shuaiqi, Xia, Sonia Phene, Spencer Papay, Srinivas Narayanan, Steve Coffey, Steve Lee, Stewart Hall, Suchir Balaji, Tal Broda, Tal Stramer, Tao Xu, Tarun Gogineni, Taya Christianson, Ted Sanders, Tejal Patwardhan, Thomas Cunninghamman, Thomas Degry, Thomas Dimson, Thomas Raoux, Thomas Shadwell, Tianhao Zheng, Todd Underwood, Todor Markov, Toki Sherbakov, Tom Rubin, Tom Stasi, Tomer Kaf-tan, Tristan Heywood, Troy Peterson, Tyce Walters, Tyna Eloundou, Valerie Qi, Veit Moeller, Vinnie Monaco, Vishal Kuo, Vlad Fomenko, Wayne Chang, Weiyi Zheng, Wenda Zhou, Wesam Manassra, Will Sheu, Wojciech Zaremba, Yash Patil, Yilei Qian, Yongjik Kim, Youlong Cheng, Yu Zhang, Yuchen He, Yuchen Zhang, Yujia Jin, Yunxing Dai, and Yury Malkov. Gpt-4o system card, 2024. 5, 14
- [28] Roni Paiss, Ariel Ephrat, Omer Tov, Shiran Zada, Inbar Mosseri, Michal Irani, and Tali Dekel. Teaching clip to count to ten. In *Proceedings of the IEEE/CVF International*

- Conference on Computer Vision (ICCV)*, pages 3170–3180, 2023. 1, 2
- [29] Ji-Hoon Park, Yeong-Joon Ju, and Seong-Whan Lee. Explaining generative diffusion models via visual analysis for interpretable decision-making process. *Expert Syst. Appl.*, 248(C), 2024. 15
- [30] Dustin Podell, Zion English, Kyle Lacey, Andreas Blattmann, Tim Dockhorn, Jonas Müller, Joe Penna, and Robin Rombach. SDXL: Improving latent diffusion models for high-resolution image synthesis. In *The Twelfth International Conference on Learning Representations*, 2024. 1, 2, 5, 6, 7, 13, 15
- [31] Alec Radford, Luke Metz, and Soumith Chintala. Unsupervised representation learning with deep convolutional generative adversarial networks, 2016. 1
- [32] Alec Radford, Jong Wook Kim, Chris Hallacy, Aditya Ramesh, Gabriel Goh, Sandhini Agarwal, Girish Sastry, Amanda Askell, Pamela Mishkin, Jack Clark, Gretchen Krueger, and Ilya Sutskever. Learning transferable visual models from natural language supervision. In *Proceedings of the 38th International Conference on Machine Learning*, pages 8748–8763. PMLR, 2021. 2, 14
- [33] Aditya Ramesh, Mikhail Pavlov, Gabriel Goh, Scott Gray, Chelsea Voss, Alec Radford, Mark Chen, and Ilya Sutskever. Zero-shot text-to-image generation. In *Proceedings of the 38th International Conference on Machine Learning*, pages 8821–8831. PMLR, 2021. 1
- [34] Royi Rassin, Eran Hirsch, Daniel Glickman, Shauli Ravfogel, Yoav Goldberg, and Gal Chechik. Linguistic binding in diffusion models: Enhancing attribute correspondence through attention map alignment. In *Advances in Neural Information Processing Systems*, pages 3536–3559. Curran Associates, Inc., 2023. 3
- [35] Douglas Reynolds. *Gaussian Mixture Models*, pages 659–663. Springer US, Boston, MA, 2009. 14
- [36] Robin Rombach, Andreas Blattmann, Dominik Lorenz, Patrick Esser, and Björn Ommer. High-resolution image synthesis with latent diffusion models. In *Proceedings of the IEEE/CVF Conference on Computer Vision and Pattern Recognition (CVPR)*, pages 10684–10695, 2022. 1, 2, 5, 6, 7, 13, 15
- [37] Chitwan Saharia, William Chan, Saurabh Saxena, Lala Li, Jay Whang, Emily L Denton, Kamyar Ghasemipour, Raphael Gontijo Lopes, Burcu Karagol Ayan, Tim Salimans, Jonathan Ho, David J Fleet, and Mohammad Norouzi. Photo-realistic text-to-image diffusion models with deep language understanding. In *Advances in Neural Information Processing Systems*, pages 36479–36494. Curran Associates, Inc., 2022. 1
- [38] Narek Tumanyan, Michal Geyer, Shai Bagon, and Tali Dekel. Plug-and-play diffusion features for text-driven image-to-image translation. In *Proceedings of the IEEE/CVF Conference on Computer Vision and Pattern Recognition (CVPR)*, pages 1921–1930, 2023. 1
- [39] Qiu Weimin, Wang Jieke, and Tang Meng. Self-cross diffusion guidance for text-to-image synthesis of similar subjects. In *CVPR*, 2025. 3
- [40] Song Wen, Guian Fang, Renrui Zhang, Peng Gao, Hao Dong, and Dimitris Metaxas. Improving compositional text-to-image generation with large vision-language models, 2023. 1
- [41] Jiazheng Xu, Xiao Liu, Yuchen Wu, Yuxuan Tong, Qinkai Li, Ming Ding, Jie Tang, and Yuxiao Dong. Imagereward: Learning and evaluating human preferences for text-to-image generation, 2023. 5, 7, 14, 15
- [42] Oz Zafar, Lior Wolf, and Idan Schwartz. Iterative object count optimization for text-to-image diffusion models, 2024. 2, 5, 6, 7, 13, 15
- [43] Ruisu Zhang, Yicong Chen, and Kangwook Lee. Zero-shot improvement of object counting with CLIP. In *RoFoMo: Robustness of Few-shot and Zero-shot Learning in Large Foundation Models*, 2023. 2

# CountCluster: Training-Free Object Quantity Guidance with Cross-Attention Map Clustering for Text-to-Image Generation

## Supplementary Material

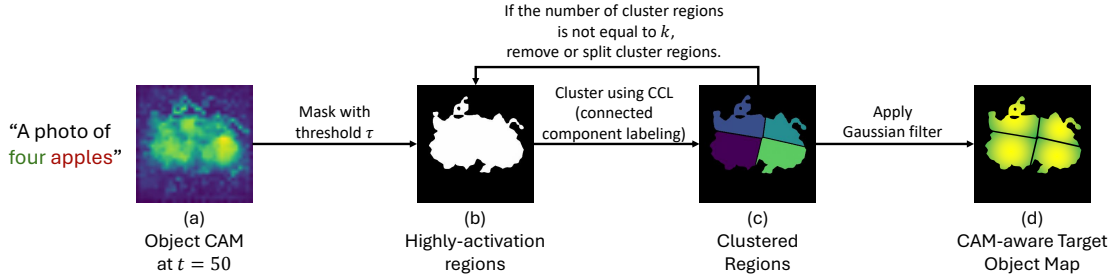


Figure 6. Overview of the CAM-aware target object map extraction process, including CAM masking, cluster formation via CCL, cluster count adjustment, and Gaussian filtering to obtain the target object map.

### A. Details of the Proposed Method

In this section, we explain the details of the proposed method. As described in the Motivation section, to generate the intended number of object instances without additional training, the object cross-attention map (CAM) needs to form distinct clusters around its high-activation regions at the initial denoising timestep. Therefore, we extract a CAM-aware target object map in which the object CAM forms clear and well-separated clusters for the intended number of objects, and then optimize the latent representation by minimizing the KL divergence between the object CAM and this CAM-aware target object map.

In CAM-aware target object map extraction, we first apply Connected Component Labeling (CCL) to the object CAM to divide it into separate regions. If the number of resulting regions exceeds the intended object count, we remove smaller regions to match the target count. In contrast, if the number of regions is smaller than intended, we split larger regions to obtain the required number. The resulting regions are converted into a continuous distribution by applying a Gaussian filter. Finally, based on the CAM-aware target object map, we optimize the latent representation using the appearance loss and the separation loss.

#### A.1. CAM-aware Target Object Map Extraction

Fig. 6 illustrates the overall process of CAM-aware target object map extraction. To construct a target map where clusters form around the originally high-activation regions, we first mask out the regions of the object CAM with activation values lower than the threshold  $\tau$ , so that only regions

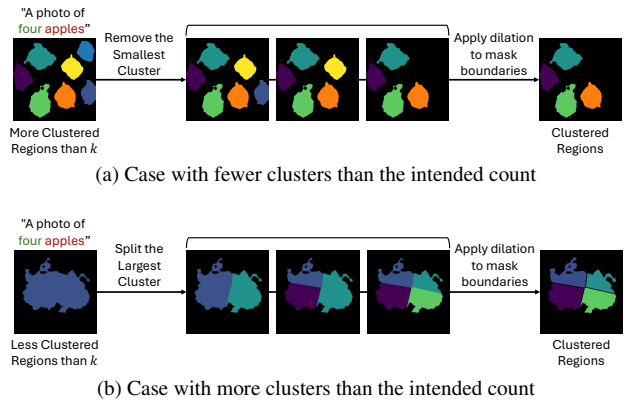


Figure 7. Cluster count adjustment process to match the intended count. (a) Case with fewer clusters than the intended count. (b) Case with more clusters than the intended count.

above  $\tau$  remain, as shown in Fig. 6 (b).

Next, we apply connected component labeling (CCL) to form the intended  $k$  separated object CAM clusters. CCL is a conventional image-processing technique that assigns distinct labels to separated activation regions based on DFS searching, enabling the extraction of separated activation clusters. However, CCL does not guarantee that the number of detected clusters matches the intended count  $k$ . Therefore, we refine the clustering output to align with the intended number of clusters, as shown in Fig. 6 (c). If the number of resulting regions exceeds  $k$ , we remove smaller clusters until the target count is reached, as illustrated in Fig. 7 (a). In contrast, if the number of regions is smaller

than  $k$ , we split larger clusters using a k-means-based partitioning process until the target count is reached, as shown in Fig. 7 (b). Through this iterative process, we obtain  $k$  well-separated cluster regions.

Based on  $k$ -clustered regions, we apply a Gaussian filter to the target map to obtain a continuous-valued target distribution. This CAM-aware target object map guides the latent optimization process for object count control.

## A.2. Latent Optimization with CountCluster Loss

Based on the extracted CAM-aware target object map, we compute the CountCluster loss, which consists of appearance and separation losses, and optimize the latent representation with our loss.

The appearance loss is defined as the KL divergence [21] between the object CAM  $A_c(x)$  and the target object map  $T_j(x)$ . Minimizing this loss encourages the object CAM to become closer to the target map, allowing it to form  $k$  clearly separated activation clusters.

The separation loss is computed as the softmax value of non-target-map regions, regions where no cluster is located. When the separation loss is minimized, the model suppresses CAM activations in non-target-map regions below the threshold  $\tau$ , which reduces unnecessary activation outside the clusters and leads to clearer separation between clusters. Using our proposed loss, we update the latent representation at the first denoising timestep.

## B. Implementation Details

### B.1. Detailed Experimental Setup

In this study, we implemented our method and determined all hyperparameters with reference to the diffusion pipeline code of Attend-and-Excite [6]. The proposed quantity control method was built on both pretrained SD2.1 [36] and SDXL [30] models. The object tokens and their quantities were automatically extracted from the prompt using the `inflect` library.

During image generation, the guidance scale [15] of the diffusion model was fixed at 7.5. In the proposed method, Gaussian smoothing with a kernel size of 3 and  $\sigma = 0.5$  was applied to the object cross-attention map, followed by min-max normalization. For the clustering step, we set the attention score threshold  $\tau = 0.35$ .

The image latent was updated during the first 10 timesteps of the denoising process ( $t = 50$ ). In ours (SD2.1), the scale factor ( $\alpha$ ) was set to 1, while in ours (SDXL), it was set to 10,000. The latent was updated 20 times in total.

For image generation, CountGen [3] utilized four NVIDIA RTX 3090 GPUs in parallel for inference, whereas all other experiments were conducted on a single RTX 3090 GPU. In addition, count token training for the method of

Zafar et al. [42] was performed using two RTX 3090 GPUs.

### B.2. Detailed Benchmark Description

For our experiments, we constructed a benchmark prompt set by integrating those proposed in Counting Guidance [18] and CountGen [3], using prompts of the form “A photo of [count] [object]”. Here, [count] is an English word from two to ten, and [object] is selected from the 19 predefined categories listed in Tab. 5.

<b>Count</b>	two, three, four, five, six, seven, eight, nine, ten
<b>Object</b>	apples, bears, birds, cars, cats, clocks, dogs, donuts, eggs, elephants, frogs, horses, lemons, mice, monkeys, onions, oranges, tomatoes, turtles

Table 5. List of counts and objects used in the benchmark set

### B.3. Evaluation Metrics

**Counting Module-based Evaluation.** To evaluate the quantity of objects in the generated images, we employed CountGD [2] to automatically measure the number of instances in each image corresponding to the object specified in the prompt. The predicted number of instances obtained from CountGD were then compared with the target counts provided in the prompts to compute the following evaluation metrics: Accuracy (Acc), Mean Absolute Error (MAE), and Root Mean Square Error (RMSE). The formulas for each metric are as follows:

$$\text{Acc} = \sum_{i=1}^n \frac{\mathbf{1}[y_i = \hat{y}_i]}{n} \quad (7)$$

$$\text{MAE} = \sum_{i=1}^n \frac{|y_i - \hat{y}_i|}{n} \quad (8)$$

$$\text{RMSE} = \sqrt{\sum_{i=1}^n \frac{(y_i - \hat{y}_i)^2}{n}} \quad (9)$$

Here,  $y_i$  denotes the target object count specified in the  $i$ -th prompt, and  $\hat{y}_i$  is the number of corresponding object instances in the  $i$ -th generated image as predicted by CountGD.  $n$  represents the total number of generated images. In our experiments, we evaluated each method on a total of 1,710 images, generated by applying 10 random seeds (0~9) to all 171 combinations of counts and objects.

**VQA-Based Evaluation.** For VQA-based evaluation, we utilize the TIFA framework [17], which utilizes GPT-4o

mini [27] as the VQA model, to jointly evaluate the Counting score and Appearing score. The TIFA score is computed as the proportion of VQA queries for which GPT-4o mini provides the correct answer based on the generated image:

$$\text{TIFA Score} = \sum_{i=1}^n \frac{\mathbf{1}[A_i = \hat{A}_i]}{n} \quad (10)$$

Here,  $A_i$  denotes the ground-truth answer for the  $i$ -th question,  $\hat{A}_i$  represents the answer generated by GPT-4o mini, and  $n$  is the total number of question-answer pairs. The question-answer pairs actually used in the TIFA framework are exemplified in Tab. 6 and Tab. 7.

<b>Prompt:</b> <i>A photo of two apples</i>
<b>Question:</b> How many apples are in the photo?
<b>Choices:</b> 1, 2, 3, 4
<b>Answer:</b> 2

Table 6. Example of Counting VQA

<b>Prompt:</b> <i>A photo of two apples</i>
<b>Question:</b> What fruit is in the photo?
<b>Choices:</b> apples, oranges, bananas, pears
<b>Answer:</b> apples

Table 7. Example of Appearing VQA

**Image Quality Evaluation.** To evaluate the quality of the generated images, we employ ImageReward [41] and CLIPScore [13]. ImageReward captures human preference for image quality. ImageReward is a reward model trained on expert preference comparisons over roughly 130,000 text-image pairs. It considers multiple aspects such as image quality, text-image alignment, and aesthetics to approximate human preference. For each prompt-image pair, the model outputs a scalar score, and higher scores mean that the image is more preferred by humans. In contrast, CLIPScore measures how well the image semantically aligns with the text. It is computed using the cosine similarity between the text embedding  $c$  and image embedding  $v$  obtained from CLIP [32]. CLIPScore is defined as:

$$\text{CLIPScore}(c, v) = w \cdot \max(\cos(c, v), 0), \quad (11)$$

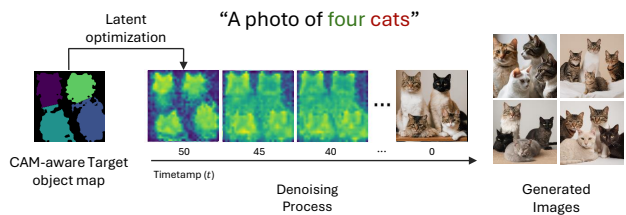
where  $w = 2.5$  is a scaling factor used to normalize the score to the  $[0, 1]$  range. Higher CLIPScore values indicate stronger semantic alignment between the generated image and the textual prompt.

Method	CountGD		
	Acc. (↑)	MAE (↓)	RMSE (↓)
GMM [35]	47.56	0.953	<b>1.674</b>
Ours	<b>55.75</b>	<b>0.821</b>	1.849

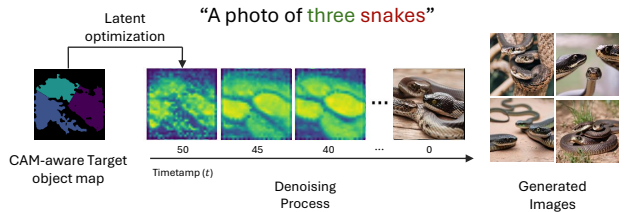
Table 8. Ablation study of GMM and CCL (ours) based target map extraction on counting accuracy.

Method	Image Quality	
	CLIPScore (↑)	ImageReward (↑)
GMM	<b>0.269</b>	0.211
Ours	0.262	<b>0.563</b>

Table 9. Ablation study of GMM and CCL (ours) based target map extraction on image quality.



(a) Objects that are closely placed or occluded



(b) Objects with non-Gaussian shapes

Figure 8. Images generated by our method under challenging scenarios. (a) Objects that are closely placed or occluded. (b) Objects with non-Gaussian shapes.

## C. Comparison of Clustering Methods for Target Map Extraction

Tab. 8 and Tab. 9 presents an ablation study that evaluates the effectiveness of the proposed CCL-based clustering strategy by comparing it with Gaussian Mixture Model (GMM) [35] clustering. It aims to verify whether explicitly leveraging the spatial connectivity of high-activation regions is more suitable for extracting reliable target object maps in proposed framework.

As shown in Tab. 8, the proposed CCL-based clustering with region count adjustment consistently achieves higher counting accuracy and better image quality than GMM-based clustering. We observe that GMM tends to form clusters around small, artifact-like local activations in the masked attention map, which do not correspond to mean-

Method	CountGD [2]			TIFA [17]	
	Acc. ( $\uparrow$ )	MAE ( $\downarrow$ )	RMSE ( $\downarrow$ )	Counting ( $\uparrow$ )	Appearing ( $\uparrow$ )
SD2.1 [36]					
Naive SD2.1 [36]	30.00	<b>1.460</b>	<b>2.126</b>	71.04	<b>82.41</b>
Counting-Guidance [18]	35.00	2.000	6.198	73.40	82.41
Ours	<b>39.50</b>	2.045	8.229	<b>74.41</b>	81.41
SDXL [30]					
Naive SDXL [30]	27.50	8.285	32.438	74.41	<b>83.42</b>
Zafar et al. [42]	16.50	4.575	12.449	72.39	73.37
CountGen [3]	44.40	3.015	10.047	77.10	82.41
Ours	<b>50.00</b>	<b>2.330</b>	<b>7.890</b>	<b>77.44</b>	82.41

Table 10. Experimental Results on Comparison of object count accuracy on T2I-CompBench Count [42] between CountCluster (Ours) and existing methods.

ingful object instances. As a result, such spurious clusters degrade both object count accuracy and overall image quality.

As shown in Tab. 9, While GMM-based clustering yields a slightly higher CLIPScore, our method achieves substantially higher ImageReward scores, indicating that the generated images are more preferred in terms of perceptual quality and visual coherence. These results suggest that explicitly leveraging the spatial connectivity of high-activation regions and filtering out artifact-level responses is crucial for reliable object count control.

## D. Analysis of Potential Concerns

We construct a 2D Gaussian-based target object map and use it to guide the object CAM at the first denoising timestep to form  $k$  clearly separated cluster regions. Under this design, the following concerns may arise: (1) Can the model reliably generate objects that are closely placed or occluded? (2) Can it properly generate objects whose shapes are not Gaussian? Figure 8 shows that our method successfully addresses these scenarios.

Our method enforces alignment between the object CAM and the target object map only at the first denoising timestep, not across all timesteps. This design is motivated by prior observations [5, 29] that core concepts of objects such as a cat’s ears or a human’s head are determined during the earliest diffusion steps. Leveraging this property, we constrain the core concept to appear only at the first timestep, while subsequent timesteps rely on the diffusion model’s inherent representational ability to generate natural object structures. It allows our method to produce high-quality images even when objects are close to each other, occluded, or have shapes that are not Gaussian.

Method	Image Quality	
	CLIPScore ( $\uparrow$ )	ImageReward ( $\uparrow$ )
SD2.1 [36]		
Naive SD2.1 [36]	0.247	0.434
Counting Guidance [18]	0.248	<b>0.532</b>
Ours	<b>0.248</b>	0.487
SDXL [30]		
Naive SDXL [30]	0.251	0.379
Zafar et al. [42]	0.239	<b>0.532</b>
CountGen [3]	0.252	0.301
Ours	<b>0.255</b>	0.368

Table 11. Comparison of image quality using CLIPScore [14] and ImageReward [41].

## E. Quantitative Results on T2I-CompBench Count

Tab. 10 and Tab. 11 shows the experimental results on the T2I-CompBench Count [3] prompt set. Compared to the integrated benchmark prompt set, this benchmark consists of prompts that specify both object counts and more complex scene compositions, making it closer to real-world scenarios. Experimental results show that the proposed method achieves the highest object count accuracy under both CountGD- and TIFA-based evaluations on this prompt set.

In terms of image quality, the SD2-based variant of our method outperforms its corresponding base model, whereas the SDXL-based variant exhibits slightly lower image quality than the base model, indicating a trade-off between counting accuracy and image quality. Notably, in this prompt set, higher ImageReward scores are often obtained when the complex object compositions specified in the text prompts are faithfully reflected in the generated images. Under this condition, our method demonstrates the ability to satisfy object composition constraints while maintaining high object count accuracy.

## **F. More Qualitative Results**

We provide additional qualitative results across a wider range of object counts and prompts. As shown in Fig. 9, existing methods often fail to match the intended number or generate instances that are not clearly distinguishable. In contrast, our method generates the correct number of instances, and the individual objects are clearly distinguishable.

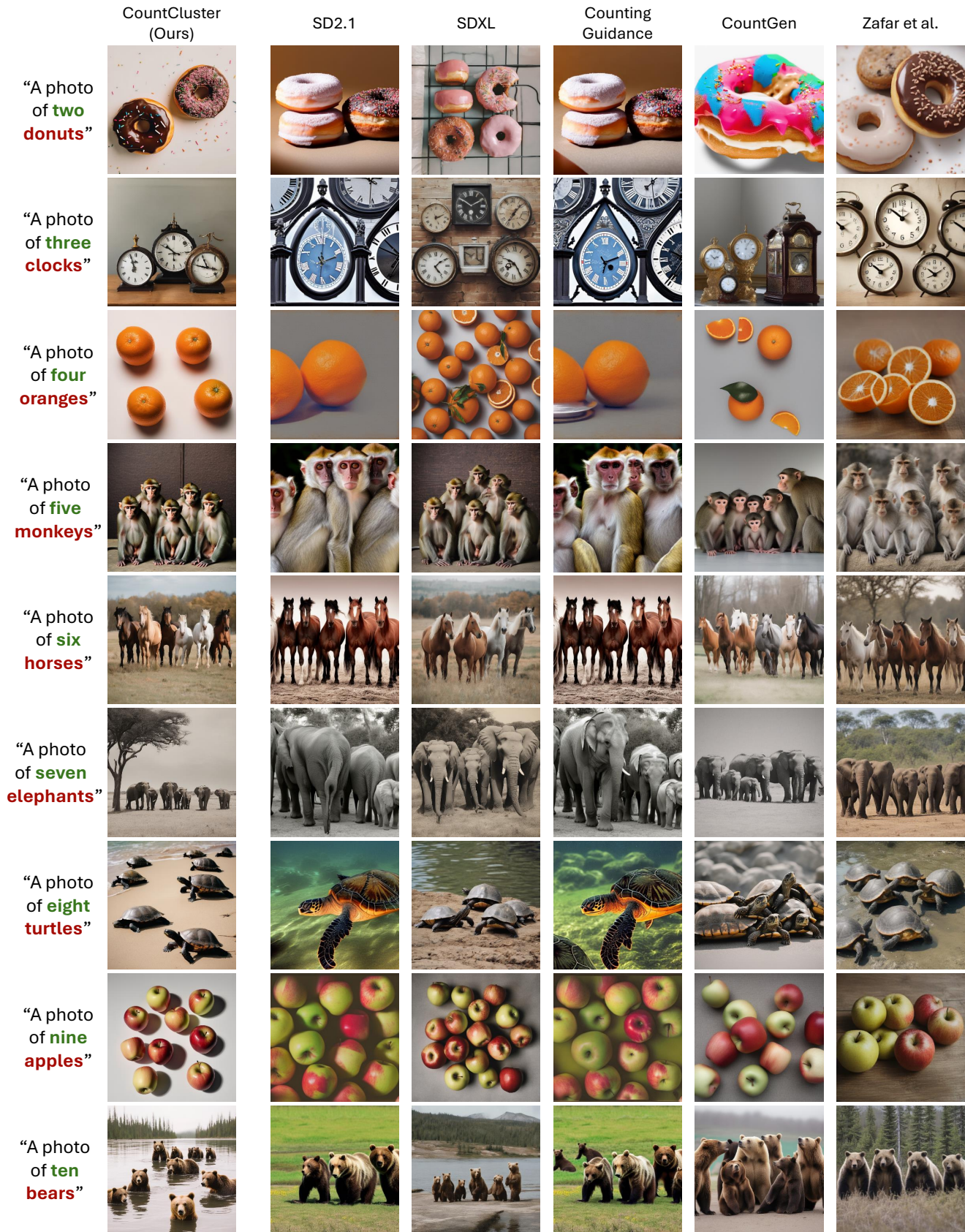


Figure 9. More qualitative comparisons between CountCluster and existing methods.